Int. J Multiphase Flow Vol 12, No 4, pp 655–666, 1986
Printed in Great Britain

0301-9322/86 $3.00 + .00
Pergamon Journals/Elsevier

INITIAL STAGES OF THE INTERACTION OF A SHOCK WAVE WITH A DUST DEPOSIT

C. C. HWANG
Department of Mechanical Engineering, University of Pittsburgh, Pittsburgh, PA 15261, U.S.A

(*Received* 28 *May* 1985, *in revised form* 18 *October* 1985)

Abstract—The trajectories of solid particles which are raised from a dust deposit after the passage of a weak shock wave are explored by computations and compared with available experiments. A dust particle experiences a lift force on account of the velocity gradient within the boundary layer behind the shock front. An analytical expression by Saffman for this lift force is used in the equation of motion for the particle. The computations show that a particle lifted beyond the shock boundary layer loses lift force, reenters the growing boundary layer, and moves toward the floor. By applying these computations to particles originated from various locations of the floor, an envelope formed by the instantaneous particle positions may simulate the dust profile in the entrainment processes of a dust deposit by a gas stream. The present model shows general good agreement with laboratory experiments under various test conditions

INTRODUCTION

The problem of small particle entrainment from the floor region into a fuid stream is encountered in many branches of science and engineering. The erosion of soil and sand by wind (Bagnold 1941; Chapil 1945) entrainment of coal particles during coal-dust explosions (Dawes 1952; Singer *et al*. 1972; Hwang *et al*. 1974), pneumatic transport of granular materials in pipes (Owen 1969; Wen & Galli 1971; Zenz 1964), and erosion of river banks by water streams (Yalin 1972) are some of the examples of particle entrainment by fluid streams. A survey of the literature reveals that the origin and mechanism of lifting dust particles from a surface by a fluid stream are still not well understood. In general, the lift has been attributed to the shear force at the bed surface. This force in turn sets particles in motion, and saltation or rolling of particles takes place (Owen 1964; Yalin 1972).

By noting the presence of velocity fluctuations (turbulent bursts) in a boundary layer, Owen (1964) suggested a mechanism of lifting dust particles by turbulent bursts. Cleaver & Yates (1973) proposed a lifting mechanism for detachment of colloidal particles from a flat substrate based on the updraft caused by turbulent bursts. Hwang & Chaiken (1975) analyzed the net upward force on the top layer of a porous medium subjected to a surface pressure oscillation. The results of the analysis indicate that the top layer of a granular bed in a turbulent stream may experience a lift as a result of turbulent bursts.

Another mode of dust-particle lifting is associated with the interaction of an air shock wave with a granular bed. This problem is mainly related to coal-mine dust explosions (Palmer 1973; Grumer 1974; Richmond & Liebman 1974). In coal-mine dust explosions, a gas stream, induced by the deflagration of combustible gas (presumably a methane-air mixture), detaches and disperses coal dust from the floor and walls of the mine entry into the flowing gas stream. If the coal-dust cloud also ignites, the explosion may sustain itself and propagate through the entry. The formation and dispersion of the coal-dust cloud ahead of the flame front are important factors which determine the subsequent flame propagation characteristics. Large scale tests on coal-dust explosions are conducted to study the overall behavior of flame propagation. In large-scale experiments, it is relatively difficult to control the parameters to investigate the entrainment and dispersal of coal particles systematically. Laboratory experiments using shock tubes (Gerrard 1963; Borisov *et al*. 1967; Fletcher 1976; Merzkirch & Bracht 1978; Bracht & Merzkirch 1979; Hwang 1982) supplemented the data from large-scale tests and helped gain more insight into the fundamental mechanisms of dust entrainment.

The fundamental problems in these laboratory experiments are to determine the origin and to predict the magnitude of the forces which cause dust particles to rise from the

channel floor into the air stream which is parallel to the initial dust layer. Gerrard (1963) attributed these forces to the flow of gas into and out of the dust layer behind the shock wave front. This explanation is based on the observation that the initially plane shock wave is curved close to the dust layer, indicating a component of air velocity towards the surface and air flowing into the dust deposit. This inward air flow is reflected from the base of the deposit, resulting in initial dust raising. Borisov *et al*. (1967) passed detonation waves (2800 m/s) and shock waves (450 m/s) over sand layers of various depths (particle diameters of 200 – 300 μm). In the case of thin layers (of the order of 0.5 mm), sand was dispersed with a wavelike profile. It was suggested that the particles were thrown upward on account of the hydrodynamic instability of the surface of the thin layer. A systematic investigation by Fletcher (1976) indicates that dust is raised as a result of the rapid flow that follows immediately behind the shock wave, rather than as a result of refraction-reflection in the dust layer. Merzkirch & Bracht (1978) computed the motion of a spherical particle in the boundary layer behind a moving shock front. They included an analytical expression for the lift force of a sphere within a shear layer (Saffman 1965). The velocity profile in the boundary layer was assumed to be sinusoidal. The results of the analysis gave good agreement with the results of their shock-tube experiments.

In the present paper, the model employed by Merzkirch & Bracht (1978) is reexamined. The model considers a boundary layer behind a shock wave. The velocity profile in the shock boundary layer is adopted from the work of Mirels (1955) for a weak shock. A dust particle experiences a lift force on account of the velocity gradient within the boundary layer. An analytical expression by Saffman (1965) for this lift force is used in the equations of motion for the particle. Trajectories of various size particles detached from a floor surface after the passage of a weak shock are computed and compared with available experimental results taken with shock tubes (Gerrard 1963; Fletcher 1976; Merzkirch & Bracht 1978; Hwang 1982). Also included are the experimental data by Emmons & Pennebaker (1957) in which dust particles are laid on the channel floor forming a single-layer deposit.

ANALYSIS

Consider a shock-tube experiment in which a plane shock wave moves in the direction parallel to the tube axis (x-axis) with a velocity U_s. As dipicted in figure 1, the origin of the x-y coordinate system is fixed at the leading edge of the dust bed, with the positive y directions measured upward from the top surface of the dust deposit which is flush with the channel floor. The stagnant gas prior to the shock-wave arrival is induced to flow behind the wave with a velocity $u_G = u_2$, the value of which depends solely on U_s and the gas type, given by (Owczarek 1964)

$$\frac{u_2}{a_1} = \frac{2}{k+1}\left(M_s - \frac{1}{M_s}\right), \qquad [1]$$

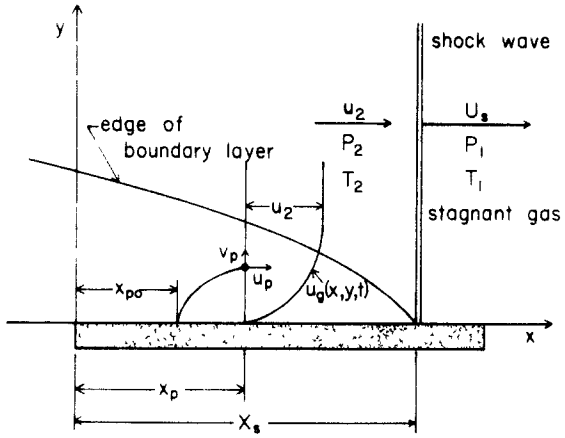

Figure 1 Coordinate system fixed at the leading edge of a dust deposit

where a_1 is the acoustic speed of the stagnant gas, k is the specific heats ratio, and M_s is the shock Mach number defined by

$$M_s = \frac{U_s}{a_1}.$$

The pressure P_2 and temperature T_2 behind the shock are calculated from

$$\frac{P_2}{P_1} = 1 + \frac{2k}{k+1}(M_s^2 - 1), \quad [2]$$

$$\frac{T_2}{T_1} = 1 + \frac{2(k-1)}{(k+1)^2}\left[k M_s^2 - \frac{1}{M_s^2} - (k-1)\right]. \quad [3]$$

At a station x, the gas velocity $u_G(t, y)$ varies across the shock-tube boundary layer which originates at the shock-wave front (Mirels 1955). For the limiting case of a weak shock, the gas velocity u_G varies with the distance from the wave front $(X_s - x)$ and the distance y from the floor surface according to

$$\frac{u_G}{u_2} = \operatorname{erf}\left[\frac{y}{2}\sqrt{\frac{U_s - u_2}{\nu(X_s - x)}}\right], \quad [4]$$

where ν is the kinematic viscosity of the gas. In the present analysis concerning the lifted particle motion, the effect of gas temperature across the boundary layer is neglected. The boundary-layer thickness can be determined by setting $y = \delta$ and $u_G/u_2 = 0.99$ in [4], yielding

$$\delta = 3.64\left[\frac{\nu(X_s - x)}{(U_s - u_2)}\right]^{1/2}. \quad [5]$$

It may be noted that u_G and δ are functions of time through $X_s = U_s t$.

The fundamental problem here is to predict the manner in which a dust particle is raised from the channel bottom surface and enters the air stream. A noted feature of the dust entrainment process is continuous alterations of the bed boundary after the initiation of the process. The change in the solid boundary in turn alters the gas flow field and, as a result, feedback processes exist between the interface and the gas flow field. For this reason, the present analysis, which is based on a fixed gas flow field without consideration of dust-bed boundary variations, is valid only for the initial period of entrainment. It will be assumed that the particle cloud has negligible disturbances on the gas velocity.

The momentum equations for a single particle with diameter D_p and mass m_p can be written as

$$m_p \frac{du_p}{dt} = F_D \frac{u_G - u_p}{\sqrt{(u_G - u_p)^2 + v_p^2}}, \quad [6]$$

$$m_p \frac{dv_p}{dt} = -m_p g - F_D \frac{v_p}{\sqrt{(u_G - u_p)^2 + v_p^2}} + F_L, \quad [7]$$

where the aerodynamic drag force F_D is given by

$$F_D = 1/2\, C_D \rho_G\, [(u_G - u_p)^2 + v_p^2]\, (\pi/4) D_p^2, \quad [8]$$

and F_L is a lift force on the particle within the shock-tube boundary layer, expressed as (Saffman 1965)

$$F_L = K\,(u_G - u_p)\left(\frac{D_p}{2}\right)^2 \left|\frac{\partial u_G}{\partial y}\right|^{1/2} (\rho_G\, \mu_G)^{1/2}, \quad [9]$$

where K is a constant. The value of C_D is a function of the particle Reynolds number Re, expressed in the form

$$C_D = \frac{k_1}{\mathrm{Re}} + \frac{k_2}{\mathrm{Re}^2} + k_3, \qquad [10]$$

where $\mathrm{Re} = (D_p/\nu)\,[(u_G - u_p)^2 + v_p^2]^{1/2}$. The values for k_is are obtained from the correlations of Morsi & Alexander (1972)

Other workers have used [9] for calculating the lift force of particles within a shear layer (Halow & Wills 1970; Soo & Tung 1971; Merzkirch & Bracht 1978). According to Halow & Wills (1970), the value of K must be multiplied by a factor of 5 to give good agreement between their measured and calculated particle trajectories. In the present computations, $K = 32.3$ is used instead of the theoretical value 6.46.

To provide appropriate scaling in numerical computations, [6] and [7] are nondimensionalized by introducing (as suggested by Merzkirch & Bracht 1978)

$$u_D = U_s - u_2, \quad u_j^* = \frac{u_j}{u_D}, \quad v_j^* = \frac{v_j}{u_D} \quad (j \text{ represents } G, p, 2 \text{ and } s)$$

$$t^* = \frac{u_D}{D_p}\,t, \quad x_j^* = \frac{x_j}{D_p}, \quad y_j^* = \frac{y_j}{D_p} \quad (j \text{ represents } G \text{ and } p)$$

$$\rho^* = \frac{\rho_G}{\rho_p}, \quad \nu^* = \frac{\nu}{(D_p u_D)}, \quad g^* = g\frac{D_p}{u_D^2},$$

$$\delta^* = \frac{\delta}{D_p},$$

to yield

$$\frac{du_p^*}{dt^*} = \frac{3}{4} C_D\, \rho^* (u_G^* - u_p^*)\,[(u_G^* - u_p^*)^2 + v_p^{*2}]^{1/2}, \qquad [11]$$

$$\frac{dv_p^*}{dt^*} = -g^* - \frac{3}{4} C_D\, \rho^*\, v_p^*\,[(u_G^* - u_p^*)^2 + v_p^{*2}]^{1/2} + \frac{3}{2}\frac{K}{\pi}\rho^*(u_G - u_p^*)\left(\nu^*\left|\frac{\partial u_G^*}{\partial y^*}\right|\right)^{1/2}. \qquad [12]$$

In addition, the following equations are employed for the particle trajectory:

$$\frac{dx_p^*}{dt^*} = u_p^*, \qquad [13]$$

$$\frac{dy_p^*}{dt^*} = v_p^*. \qquad [14]$$

Equations [11] – [14] are numerically integrated with the initial conditions for a particle situated at some distance from the dust-bed leading edge:

$$x_p^* = x_{p0}^*, \quad y_p^* = 0.5, \quad u_p^* = 0, \quad v_p^* = 0 \text{ at } t^* = t^*_{\mathrm{act}}.$$

The time t^* is reckoned from the instant the shock wave arrives at $x^* = 0$. The gas flow at the initial particle position commences at $t_0^* = x_{p0}^*/U_s^*$, whereas it is assumed that the fluid dynamic forces do not act on the particle until the boundary layer thickness becomes one particle diameter, i.e.,

$$\delta^* = 1.0 = 3.64\,[\nu^* U_s^*\, t^*]^{1/2},$$

from which

$$t_\delta^* = 0.0755\,(\nu^*\,U_s^*)^{-1}\,.$$

Therefore

$$t_{act}^* = t_0^* + t_\delta^*\,.$$

To be consistent with the above assumption (the particle immersed in the boundary layer), the initial value for y_p^* is set to 0.5 and not 0. This procedure is also necessary to avoid singularities in the evaluation of C_D and F_L.

RESULTS OF COMPUTATIONS

The present analysis assumes a laminar boundary layer behind the shock front and negligible erosion in the dust bed. Since the boudary layer tends to become turbulent and the dust-bed erosion commences as particles are lifted, the model is valid for an initial period of air-dust bed interaction. Although it is not possible to determine exactly the duration in which the analysis is valid, high-speed photographs indicate that there is no excessive dust-bed erosion during the initial 2 ms of interaction. It may be noted that the present model is valid for a single particle lifted behind a weak shock wave, as long as the shock boundary layer is laminar.

The trajectory of a lifted particle up to 2 ms is shown in figure 2 for the shock Mach numbers of 1.05, 1.15, and 1.44. The axial distance traveled by the particle increases more than ten folds as the shock Mach number is increased from 1.05 to 1.44. The major factors contributing to the distance traveled are the shock-induced air velocity u_2 and the air density ρ_G, shown in table 1, both of which tend to increase the drag force on the particle. The effect of the shock Mach number on the particle height is mainly through the change in the velocity gradient in the boundary layer (in fact, the square root of the velocity gradient). The particle altitude and the boundary-layer thickness (defined by [5]) at the particle position as functions of time (t_{act}) are shown in figure 3 for three values of the shock Mach number. The vertical component of the net force on particles (as expressed by the curvatures of plots d^2y_p/dt^2 in figure 3) is largest initially, decreases as the particle is raised through the gas boundary layer, and changes its direction after the particles are lifted beyond the edge of the boundary layer. The time for the particle to cross the outer edge of the boundary layer is earlier for a higher shock Mach number because of a larger initial vertical particle velocity.

The vertical particle velocity is shown in figure 4 as a function of time for three values of shock Mach number. Plots of the axial particle velocity are shown in figure 5, along with the free stream velocity u_2. It is seen that a particle approaches closer to the free-stream velocity for a high shock Mach number than for a low shock Mach number (at $t = 2$ ms, $u_p/u_2 = 0.94$ for $M_s = 1.44$ and $u_p/u_2 = 0.68$ for $M_s = 1.05$).

The effect of the particle diameter D_p is shown in figure 6 in terms of the particle altitude y_p as a function of time. For the same shock Mach number ($M_s = 1.15$ in figure 6), the boundary-layer thicknesses at the particle positions of different size are practically the same. A smaller particle (say 1 μm particle) is raised beyond the boundary layer in less time than a larger particle (say 30 μm particle). The present model predicts that the lifted particles reenter the growing boundary layer and move toward the bottom surface. In effect,

Table 1 Parameters behind air shock waves

M_2	T_2 (K)	P_2 (Pascal)	ρ_G (kg/m^3)	u_2 (m/s)	ν_G (m^2/s)
1 05	310	0.110×10^6	1.24	28 2	0.1066×10^{-4}
1.15	329	0.135×10^6	1.43	81.1	0.1066×10^{-4}
1 44	384	$0\,221\times10^6$	2.00	216	0.1066×10^{-4}

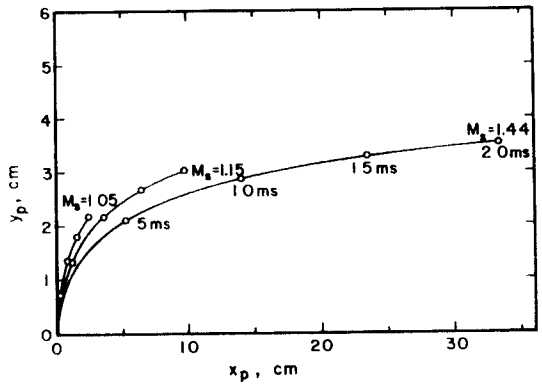

Figure 2 Trajectories of lifted particles for M_s = 1.05, 1.15, and 1.44 D_p = 30 μm, ρ_p = 1400 kg/m^3, x_{p0} = 0 m

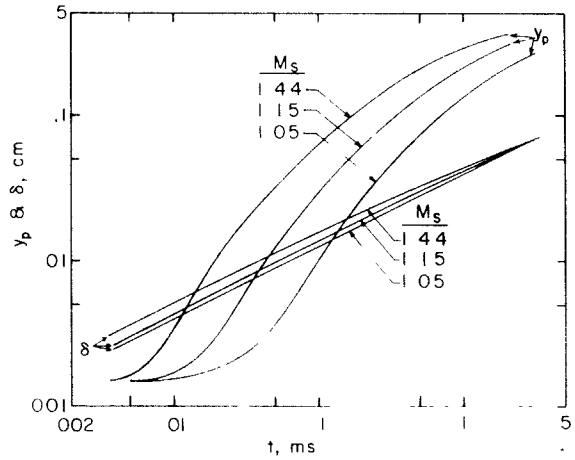

Figure 3 Particle altitude y_p and the boundary-layer thickness δ at the particle axial position as functions of time D_p = 30 μm, ρ_p = 1400 kg/m^3

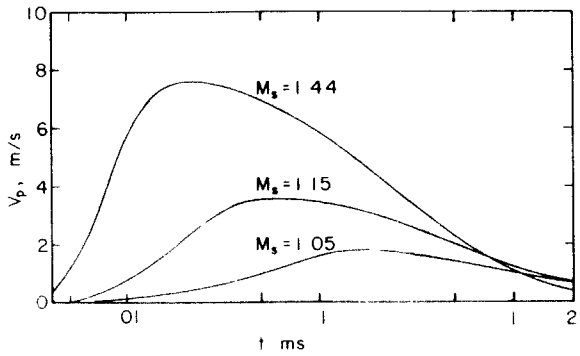

Figure 4 Vertical velocity of particle v_p as a function of time M_s = 1.05, 1.15, and 1.44 D_p = 30 μm, ρ_p = 1400 kg/m^3

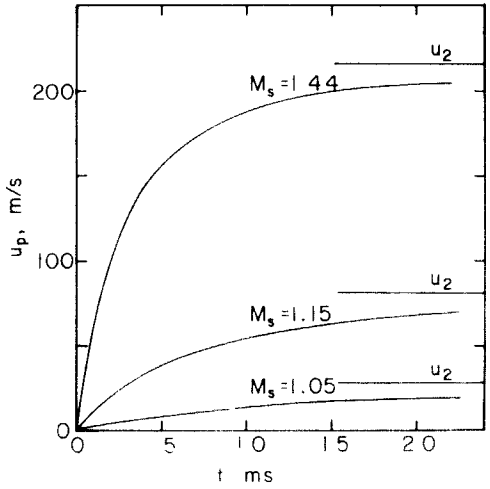

Figure 5 Longitudinal velocity of particle u_p as a function of time u_2 = 258, 216 m/s for M_s = 1.05, 1.15, and 1.44, respectively D_p = 30 μm ρ_p = 1400 kg/m^3

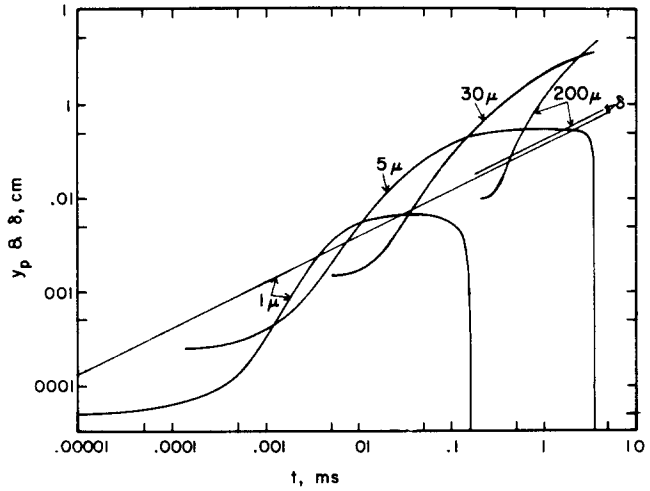

Figure 6 Particle altitude y_p and the boundary-layer thickness δ as functions of time. $D_p = 1$, 5, 30, and 200 μm. $M_s = 1.15$, $\rho_p = 1400$ kg/m^3.

the fast-growing boundary layer engulfs the particles which start decelerating after being lifted beyond the boundary layer. The particles reentering the boundary layer (1 μm and 5 μm particles are shown in figure 6) move at close to the free-stream velocity. As a result, the particle within the boundary layer moves faster than the local gas velocity and is subjected to a negative lift force. (See [9].) The particle vertical velocity v_p for different size particles is plotted as a function of time in figure 7. It is seen that a small particle suffers a significant change in the vertical velocity in a shorter time than a large particle.

The effect of particle density is shown in figure 8 for the positions of a 30 μm particle at the end of 2 ms for three values of shock Mach number and various particle densities (the density of water is 1000 kg/m^3). For $\rho_p = 1400$ kg/m^3, the particle positions at $t = 2$ ms for $M_s = 1.05$, 1.15, and 1.44 are shown in figure 2. It is seen that the particle density which attains the maximum altitude shifts from approximately 7000 kg/m^3 for $M_s = 1.44$ to 1400 kg/m^3 for $M_s = 1.05$.

SHOCK-TUBE EXPERIMENTS

To access the validity of the theoretical computations, some available results of shock-tube experiments are compared with the theory. Gerrard (1963) employed a 6 in. × 1½ in. shock tube using air as the working and driving gas. The tube was 13½ ft long and closed at one end. The diaphragm was 12 ft from the closed end and the high-pressure section

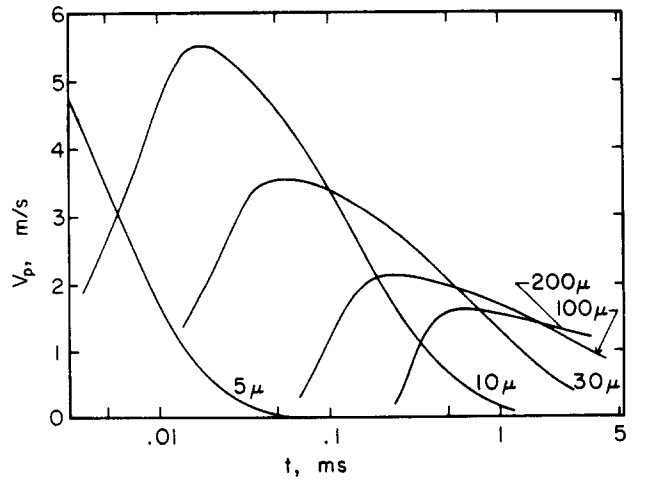

Figure 7 Effect of particle diameter D_p on v_p. $M_s = 1.15$, $\rho_p = 1400$ kg/m^3

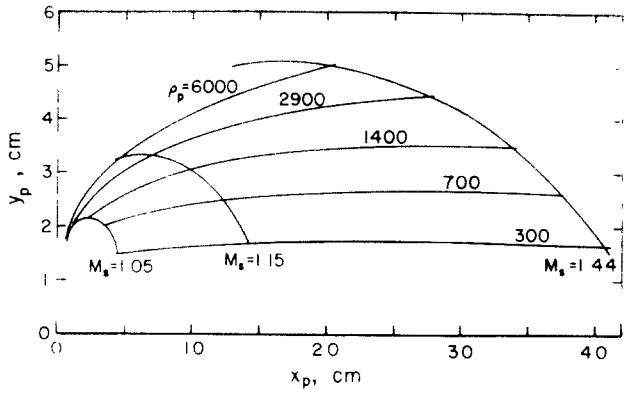

Figure 8. Effects of particle density ρ_p kg/m^3, and shock Mach number M_s on particle positions at $t = 2$ ms Effect of M_s alone is shown in figure 2.

was maintained at atmospheric pressure. The required pressure across the diaphragm was achieved by evacuating the low-pressure section of the shock tube. The dust was deposited on a flat plate spanning the working section. The trough was $1\frac{3}{8}$ in. wide and $3\frac{1}{2}$ in. long. Its depth was varied from 0.104 to 1.270 cm. The dust was precipitated carbonate with a density of 2360 kg/m^3 and particle size of 2.5 – 55 μm. Figure 9 shows a comparison of Gerrard's experimental results with the computations based on the present theory. Although the computations show general agreement with the experiment, the experiment indicates that the particle height y_p is approximately independent of the shock Mach number M_s, while the theory predicts a dependence of y_p on M_s.

Fletcher (1976) used a treated (free-flowing) limestone in a trough 88 mm wide and 760 mm long in his shock-tube experiment. The depth of the layer was varied from 3.2 to 22.4 mm in steps of 3.2 mm. Figure 10 shows his experimental results in terms of the particle height y_p versus the distance between the shock front and the longitudinal particle position $X_s - x_p$. The experimental results indicated that the profile of the dust cloud was independent of the depth of the dust layer for the range of depths used.

Merzkirch & Bracht (1978) and Bracht (1978) employed a shock tube with rectangular cross section of 40 × 60 mm in their experiment. A cavity in the floor of the test section 300 mm long is filled with dust, the kind which is normally utilized in fire extinguishers and which has a size distribution similar to that of coal dust. A comparison of one set of their experimental results with the present calculation is shown in figure 11. For a dust deposit consisting of various particle sizes, if one assumes that the dust cloud is formed by those particles which attain the maximum height, then the envelope of the trajectories in

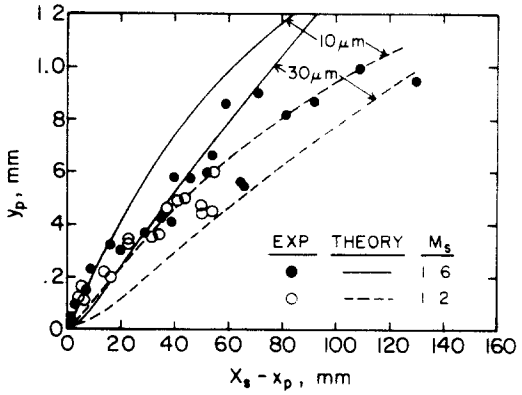

Figure 9 Comparison of the present computations with Gerrard's experimental results (1963) 2 5 μm < D_p < 55 μm

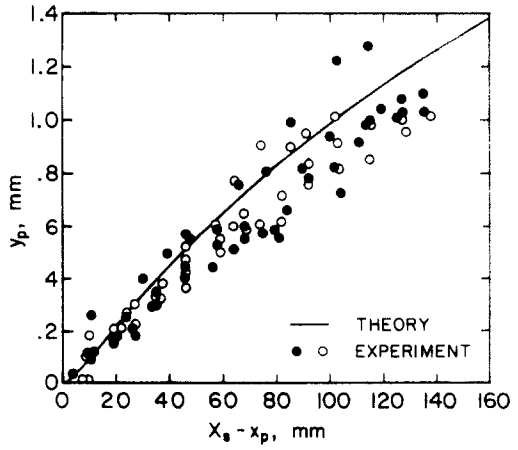

Figure 10 Comparison of the present computations with Fletcher's experimental results (1976) M_s = 1.26 Treated (free flowing) limestone, ρ_p = 2500 kg/m^3, D_p = 14 μm Depth of dust layer. (○) 6 4 mm, (●) 9 6 mm

figure 11 represents the cloud profile. The theory appears to agree well with the experimental data at an initial period but underpredicts progressively the cloud height as the value of $X_s - x_p$ increases.

Hwang (1982) employed a shock tube with a test section of 65 × 62 mm cross section. A cavity, 51 × 127 mm, in the floor of the test section was filled with coal dust (ρ_p = 1400 kg/m^3, D_p < 60 μm). A set of experimental results is shown in figure 12, along with results of computations for particle sizes ranging from 5 to 200 μm. It is seen that for this particular set of conditions, the trajectories for particles from 5 to 60 μm provide the envelope which can be interpreted as the cloud profile.

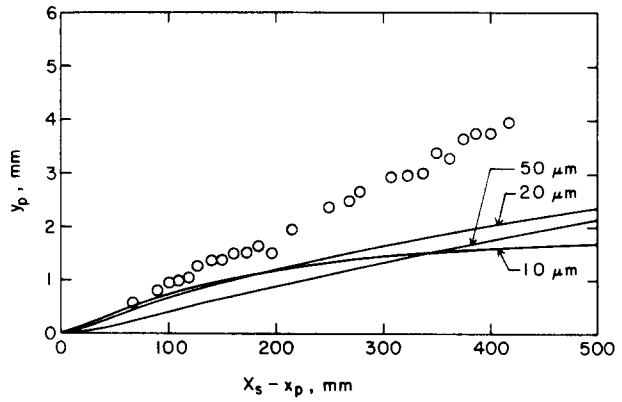

Figure 11 Comparison of the present computations with the experimental results of Merzkirch & Bracht (1978). M_s = 1.12, ρ_p = 2900 kg/m^3, D_p < 40 μm.

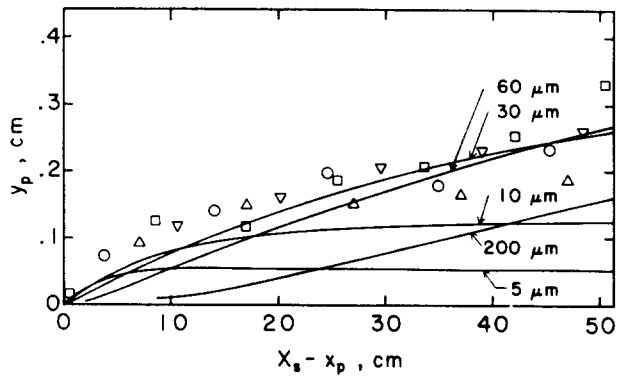

Figure 12. Comparison of the present computations with Hwang's experimental results (1982) M_s = 1.15, u_2 = 80 m/s, ρ_p = 1400 kg/m^3, D_p < 60 μm. Measured station from the leading edge of dust deposit: (○) 67 mm, (△) 30 mm, (▽) 82 mm, (□) 80 mm.

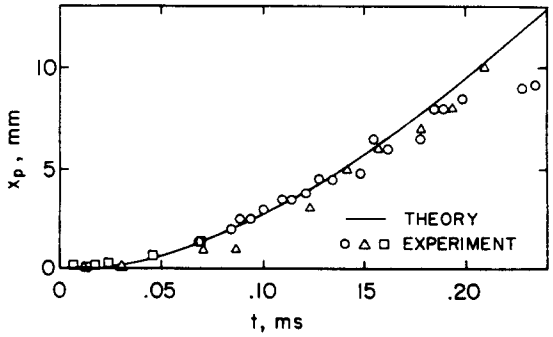

Figure 13. Comparison of the present computations with the experimental results of Emmons & Pennebaker (1957). M_s = 1.27, u_2 = 140 m/s; lycopodium particle, ρ_p = 600 kg/m^3, D_p = 30 μm. (○) dust pile, shadow pictures; (△) dust line, shadow pictures; (□) microscope in the horizontal position.

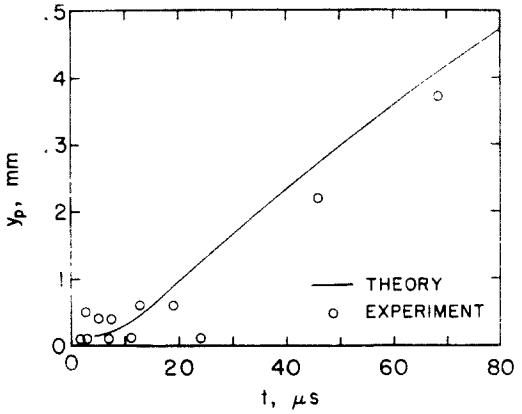

Figure 14 Comparison of the present computations with the experimental results of Emmons & Pennebaker (1957) $M_s = 1.27$, $u_2 = 140$ m/s, lycopodium particle, $\rho_p = 600$ kg/m^3, $D_p = 30$ μm

Emmons & Pennebaker (1957) performed a series of experiments in which dust particles were placed directly (monolayer) on the floor of the test section. Lycopodium powder of 30 μm diameter was employed. The test section of the shock tube was a 3 × 0.25 in. cross section. Figure 13 shows the longitudinal particle position x_p versus the elapsed time. It may be noted that the data on x_p cannot be obtained from a deposit in a trough which forms a particle cloud. The vertical particle position as a function of elapsed time after the shock arrival is shown in figure 14. In the computations shown in figures 13 and 14, the density of lycopodium is assumed to be 600 kg/m^3. The density cited in the literature ranges from 500 to 1050 kg/m^3. The agreement between the computations and experiments is good.

ADDITIONAL RESULTS OF COMPUTATIONS

A sequence of dust entrainment processes and the ensuing dust cloud profiles can be observed by means of a high-speed movie. Initially, the dust-bed surface is flush with the bottom surface of the test section. After the shock front passes, the bed surface appears bulging, the height of which increases gradually from the leading edge. The contour of the dispersed dust particles increases with time. To simulate this contour which varies with time, the trajectories of a given size particle lifted by a shock wave are calculated for various initial positions x_{p0} using the common time t_{act}, time zero being the instant the shock front passes the leading edge of the dust bed. Figure 15(a) shows the results of such calculations for 30 μm particles, with lines connecting the particle positions (solid circle) at times 0.5, 1.0, and 1.5 ms. Note that the vertical scale is 10 times the horizontal scale to show the details of particle trajectories. Similar calculations are made for other particle sizes, and

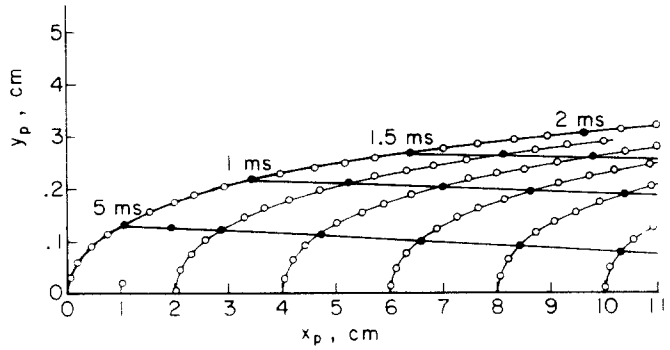

Figure 15(a) Trajectories of particles lifted by a shock wave from various initial positions $M_s = 1.15$, $D_p = 30$ μm, $\rho_p = 1400$ kg/m^3. The particle positions after 0.5, 1.0, 1.5, and 2.0 ms are shown with solid circles

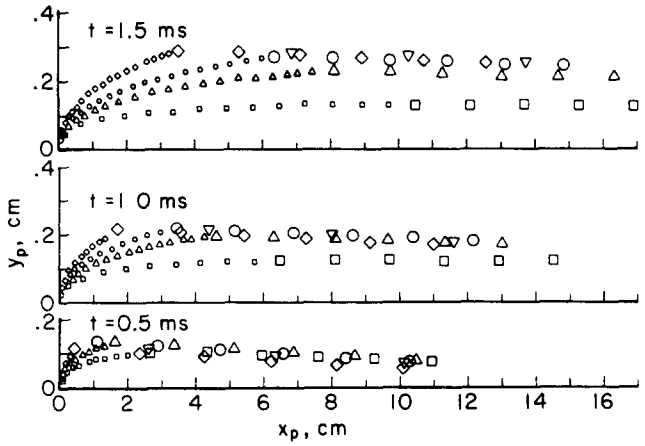

Figure 15(b) Positions of various size particles lifted by a shock wave from various initial positions. $M_s = 1.15$, $\rho_p = 1400$ kg/m^3. (◇) 60 μm, (▽) 40 μm, (○) 30 μm, (△) 20 μm, (□) 10 μm

the superpositions at times 0.5, 1.0, and 1.5 ms are shown in figure 15(b). The profiles for the initial period [say, up to 1 ms for the middle figure in figure 15(b)] are formed by the particles raised at the leading edge of the deposit but at a subsequent time ($0 < t < 1$ ms). The difference between this profile and the profile formed by the trajectory of the particle raised immediately after the shock passage is small. The profile formed by the latter case is shown in figure 15(b). If the particle interferences on each other and on the gas flow are negligible, as assumed in the present model, the profile drawn along the maximum altitude in the superimposed plots at a given time represents the height of the dust layer at that time.

CONCLUSIONS

The dispersal of particles from a dust deposit by a passage of a weak shock wave is modeled by single particles lifted at various locations passed by the shock wave. The lift force, which is based on the analytical expression by Saffman (1965) for a sphere moving relative to a shear flow, appears to adequately describe the upward motion of a solid particle within the boundary layer behind the shock front. Comparisons between the computations and dispersion experiments using the shock tube appear to confirm the validity of the present model.

Acknowledgments —The support by the National Science Foundation (Grant ENG73-08162A01, Fluid Mechanics Division) for performing the shock-tube experiments is gratefully acknowledged. Mr. S. Pillay helped run the shock-tube experiments. The author is indebted to Professor W. Merzkirch of Ruhr-Universitat and Professor R. J. Emrich of Lehigh University for making theses (Bracht's dissertation and thesis by Emmons & Pennebaker) available to him.

REFERENCES

BAGNOLD, R. A. 1941 *The Physics of Blown Sands and Desert Dunes*. Methuen, London.

BORISOV, A. A., LYUBIMOV, A. V., KOGARKO, S. M. & KOZENKO, V. P. 1967 Instability of the surface of a granular medium behind sliding shock. *Combustion, Explosion and Shock Waves* **3**, 149–151.

BRACHT, K. 1978 Eine untersuchung zur zeitlichen und ortilichen entwicklung eines gas-staub gemisches in einer stoβinduzierten stromung. Doktor-Ingenieur Dissertation, Ruhr Universität Bochum.

BRACHT, K. & MERZKIRCH, W. 1979 Dust entrainment in a shock-induced, turbulent air flow. *Int. J. Multiphase Flow* **5**, 301–312.

CHAPIL, W. S. 1945 Dynamics of wind erosion. *Soil Sci.* **60**, 397–411.

CLEAVER, J. W. & YATES, B. 1973 Mechanism of detachment of colloidal particles from a flat substrate in a turbulent flow. *J. Colloid Interface Sci.* **44**, 464–474

DAWES, J. G. 1952 Dispersion of dust deposits by blasts of air, part I Safety in Mines, Res. Est. Res. Rept. No 36

DAWES, J. G. 1952 Dispersion of dust deposits by blasts of air, part II Safety in Mines, Res. Est. Res. Rept. No. 49

EMMONS, L. B. & PENNEBAKER, W. B. 1957 An investigation of dust pickup and transport in a shock tube. B.S. Thesis, Lehigh University.

FLETCHER, B. 1976 The interaction of shock with a dust deposit. *J. Phys. D: Appl. Phys.* **9**, 197–202.

GERRARD, J. H. 1963 An experimental investigation of the initial stages of the dispersion of dust by shock waves. *Brit. J. Appl. Phys.* **14**, 186–192.

GRUMER, J. 1974 Recent research concerning extinguishment of coal dust explosions. 15th Symposium (International) on Combustion, pp. 103–114, The Combustion Institute, Pittsburgh, PA.

HALOW, J. S. & WILLS, G. B. 1970 Radial migration of spherical particles in Couette system. *AIChE J.* **16**, 281–286.

HWANG, C. C. 1982 Interaction of coal-dust beds with shock-induced air stream, in *Flow Visualization II* (Edited by W. Merzkirch), pp. 547–551. Hemisphere, Washington.

HWANG, C. C. & CHAIKEN, R. F. 1975 Force on the top layers of a porous medium subjected to surface pressure oscillation. *J. Appl. Phys.* **46**, 2976–2980.

HWANG, C. C., SINGER, J. M. & HARTZ, T. N. 1974 Dispersion of dust in a channel by a turbulent gas stream. U.S. Bureau of Mines Rep. Invest. 7854.

MERZKIRCH, W. & BRACHT, K. 1978 The erosion of dust by a shock wave in air: Initial stages with laminar flow. *Int. J. Multiphase Flow* **4**, 89–95.

MIRELS, H. 1955 Laminar boundary layer behind shock advancing into stationary fluid. NACA Tech. Note 3401

MORSI, S. A. & ALEXANDER, A. J. 1972 An investigation of particle trajectories in two-phase flow systems. *J. Fluid Mech.* **55**, 193–208.

OWCZAREK, J. A. 1964 *Fundamentals of Gas Dynamics*. International Textbook, Scranton, PA.

OWEN, P. R. 1964 Saltation of uniform grains in air. *J. Fluid Mech.* **20**, 225–242.

OWEN, P. R. 1969 Pneumatic transport. *J. Fluid Mech.* **39**, 407–432.

PALMER, K. N. 1973 *Dust Explosions and Fires*. Chapman and Hall, London.

RICHMOND, J. K. & LIEBMAN, I. 1974 A physical description of coal-mine explosions. 15th Symposium (International) on Combustion, pp. 115–126, The Combustion Institute, Pittsburgh, PA.

SAFFMAN, P. G. 1965 The lift on a small sphere in a slow shear flow. *J. Fluid Mech.* **22**, 385–400.

SINGER, J. M., COOK, E. & GRUMER, J. 1972 Dispersal of coal- and rock-dust deposits. U.S. Bureau of Mines Rep. Invest. 7642.

SOO, S. L. & TUNG, S. K. 1971 Pipe flow of suspensions in turbulent fluid. Electrostatic and gravity effects. *Appl. Sci. Res.* **24**, 83–97.

WEN, C. Y. & GALLI, A. F. 1971 Dilute phase systems, in *Fluidization* (Edited by J. F. Davidson and D. Harrison) Chap. 16, Academic, New York.

YALIN, M. S. 1972 *Mechanics of Sediment Transport*, Pergamon, New York.

ZENZ, F. A. 1964 Conveyability of materials of mixed particle size. *Ind. Engng. Chem. Fundam.* **3**, 65–75.